The underground application of magnetic resonance soundings

J. M. Greben, R. Meyer and Z. Kimmie

CSIR, PO Box 395, Pretoria 0001, South Africa

Abstract

The potential application of MRS technology in locating waterbearing fractures in underground mines is studied. The determination of the presence of water ahead of mining is important to prevent accidents and to ensure higher efficiency in mining operations. In the usual surface based measurements, with horizontal loop and water layer, the geometry of the problem can be summarized by the value of the inclination of the Earth magnetic field. For MRS measurements under the geometric conditions associated with underground mining, where the loop is non-horizontal, the geometry can be expressed in an effective inclination that can be expressed in terms of the Earth magnetic inclination and declination, together with two further parameters that characterize the orientation of the mine wall. There is a geometric enhancement of the MRS signal under typical mining conditions for the locations studied. However, the loop size is severely restricted in underground conditions, limiting the feasible target depth. We therefore also looked at higher order terms in the wave number, which become relatively more important for smaller loop sizes. The consequences of the fractured hard rock aquifer conditions, typical of deep mining or tunnelling environments, are also examined. The overall conclusion is that underground MRS applications present severe technical challenges and require favorable local circumstances to be feasible at the current state of technology.

Key words: Magnetic Resonance Sounding, low water content, in-mine application

1 Introduction

Nuclear Magnetic Resonance (NMR) has become increasingly popular as a tool in hydro-geophysics and when used as a non-invasive geophysical technique to

Email address: jgreben@csir.co.za, meyer567@gmail.com, zkimmie@csir.co.za (J. M. Greben, R. Meyer and Z. Kimmie).

detect and quantify underground water (referred to as Magnetic Resonance Sounding or MRS), has become a new geophysical research area (Legchenko and Valla, 2002; Legchenko et al., 2002; Lubczynski and Roy, 2004). In this study the feasibility of using this method in the detection of water to facilitate safe underground mining and tunnelling operations is investigated. The early detection of large quantities of groundwater ahead of underground mining or tunnelling operations can be of substantial benefit. Not only may this prevent accidental flooding with its associated safety risks, but it can also substantially improve operational efficiency.

In view of the importance of the mining industry in southern Africa, it is of great significance to prevent this accidental flooding in mining operations. The extent of this industry is due to the presence of vast mineral resources in the region. In the case of gold mines mining is conducted at depths in excess of four kilometers. Parts of the Witwatersrand Goldfields are overlain by up to two kilometers of fissured and karstified dolomitic rocks that, because it is host to excessive volumes of groundwater, exerts huge hydraulic pressures in the underlying mining area. This is a serious risk to the mining environment (Wolmarans (1986); Schweitzer and Stephenson (1999)). As a result of structural deformation, a dense network of faults and fractures has created a hydraulic connection between the mining area and the overlying aquifer. Despite precautionary measures, uncontrollable water inflows into mining areas have occurred in the past, often resulting in devastating consequences and loss of life (Wolmarans (1986)). Detecting the presence of water ahead of a vertical mining or tunnelling face, and thereby negating the need for expensive cover drilling (a term used in the mining industry to describe exploratory drilling to test for the presence of water), could impact positively on the safety and cost efficiency of these operations. In mines, where hazardous water and/or gas conditions are known to occur, cover drilling is used to investigate the virgin block up to 100 m ahead of mining (Schweitzer and Stephenson (1999)). This current practice of cover drilling is normally effective in locating such fractures, but at great cost and interruption of mining progress. This motivated investigating the possibility of detecting water ahead of mining via the non-invasive MRS technique.

Performing MRS in southern Africa presents considerable challenges for three main reasons: low Earth magnetic field; low water content in fractured rock aquifers and high electromagnetic noise. In underground conditions a further complication is the fact that the size of the T_x/R_x loop is limited by the tunnel dimensions - typically 3 m by 3 m - thus reducing the depth penetration of the technique (the experience that penetration depth is roughly equal to the diameter of the loop is discussed in Lange and Yaramanci (2005)). However, given the value of the magnetic inclination, preliminary analyses indicated that there could be a substantial increase in the size of the signal due the different orientation of the loop in underground circumstances. Another effect of the

small loop size had to be considered, as well. Terms in the signal amplitude which are higher order in the wave number become more important for small loop size (or more precisely for higher ratios of z/a, where z is the penetration depth and a is the loop size) and thus may influence the measurements. To our knowledge, such terms have not been investigated before, and their study would thus be of interest in their own right. Knowing their form and magnitude allows one to improve the quality of MRS analyses.

In the usual surface application, the horizontal nature of the T_x/R_x loop and water layer results in a signal amplitude whose geometric dependence can be reduced to a dependence on the Earth geomagnetic inclination only. Underground mining is advancing along horizontal tunnels, implying vertical mine walls. Thus in order to detect water ahead of the mine face the loop will be placed vertically against the face. If we then assume that the water layers are still parallel to the loop (in other words contained in vertical fractures parallel to the mine face), then the geometry of the underground situation is basically a simple rotation of the surface application. In this case we can replace the inclination of the surface application by an effective inclination, which now depends both on the Earth geomagnetic inclination and declination, as well as on two further parameters, characterizing the orientation of the mine wall. Expressions for this effective parameter are given in the paper. Most current modelling or interpretation software does not cater for these non-surface situations. Hence, it is of considerable importance to provide the expression for the effective inclination, and to study the effects of geometry on the signal strength.

The case where the surface is sloping at low angles with respect to the Earth surface has been investigated in two recent papers (Girard et al., 2008; Rommel et al., 2006). However, these studies deviate from the assumptions made above, so that their case does not represent a straight rotation of the surface case. Hence, different approximations are made to calculate the signal amplitudes under these generalized conditions. The nature of these approximations forces them to limit the applications to small sloping angles. Our geometry constitutes a much more radical departure from the surface application. However, by assuming that the water layers, associated with vertical fracture zones, are parallel to the loop we can simplify the geometry.

We use our theoretical analysis to make a comparison of the signal strengths for synthetic data in a number of locations (South Africa, Germany and Canada), and for a number of geometrical configurations of the mine wall and pulse moments. The results confirm the enhancement of the signal in the mine-wall case for low depth penetration, however, for higher values of z/a the effect diminishes.

2 Calculation of MRS signals in underground applications

MRS is the only known scientifically based non-invasive geophysical method capable of assessing groundwater resources. Following on the original patent by Varian (Varian, 1962), and the work by Semenov and co-workers (Semenov, 1987), the method has been developed extensively in subsequent years. The method has been applied mainly, but not exclusively, to primary aquifers to assess their water content and aquifer parameters. Articles by (Legchenko et al., 2002), (Roy and Lubczynski, 2003) and (Yaramanci et al., 2002) provide good descriptions and extensive references to the application of the method to surface based groundwater exploration, while papers by (Weichman et al., 2000, 2002) deal with theoretical aspects in detail.

The method is based on the excitation of hydrogen nuclei ($^1H^+$) in groundwater through energizing a transmitter coil (T_x) on the Earth's surface with an alternating current tuned to the local precessing frequency (the Larmor frequency) of the hydrogen nuclei. The Larmor frequency, which is directly proportional to the local value of the Earth's magnetic field, is around 1200 Hz in Johannesburg, South Africa. If groundwater is present, energizing the coil at this frequency causes excitation (precessing) of hydrogen nuclei, and when the current is switched off the nuclei return to their stable orientation. The signal strength depends on the number of hydrogen nuclei present (directly proportional to the water content). The shape of the resulting decay curve as a function of time contains information on the underground water content. The transmitter coil is also used as receiver (R_x) to record the signal produced by the return of the nuclei to the ground state. By energizing the coil with different current strengths for a fixed time period (called the pulse moment q = current $\times$ pulse length) and recording the signal decay for each pulse moment, a sounding curve is produced. This sounding curve is analysed in terms of its amplitude, frequency and phase and provides information on the subsurface free water content with depth.

Various descriptions of the theory of MRS in its application to waterbearing geological structures exist (Legchenko and Valla, 2002; Weichman et al., 2000). We will review this theory with an emphasis on the geometrical aspects. As is the case in surface based MRS, it is assumed that the aquifer surface (or water filled fracture zone) is parallel to the plane of the T_x/R_x loop. Although fractures can have multiple orientations, large fracture and fault zones that are nearly vertical are commonly found in deep South African mines. The inclination ($\approx -60^0$) and declination ($\approx -17^0$) of the Earth's magnetic field in South Africa are substantially different from those encountered in the Northern hemisphere, so that it is of value to understand quantitatively how this aspect influences the applicability of MRS in the Southern hemisphere. In addition, in its application to mining, the geometries encountered are en-

tirely different again. Since, the existing inversion MRS software often does not allow the user to take into account the particular dependence on these geometrical aspects, we will discuss the relevant geometrical relations explicitly, and comment on the major differences between different applications.

Legchenko and Valla (2002) give the following expression for the induced voltage $E(t)$:

$$E(t) = -\int_V \mathrm{d}^3x\, \omega_0\, M_0\, w(\vec{x})\, b_\perp^{R_x}(\vec{x})\, \sin\left(\tfrac{1}{2}\gamma b_\perp^{T_x}(\vec{x})q\right)\, \mathrm{e}^{-t/T_2^*(\vec{x})}\ , \qquad (1)$$

where:

$\vec{x}$	=	spatial coordinate with origin at the centre of the loop
ω_0	=	Larmor frequency $= \gamma\,\lvert\mathbf{B}_0\rvert$
$\mathbf{B}_0$	=	Earth's magnetic field
γ	=	proton gyromagnetic ratio
M_0	=	nuclear magnetisation for protons in water
$w(\vec{x})$	=	water content distribution
$b_\perp^{T_x}(\vec{x})$	=	normalized perpendicular component of the magnetic induction
$b_\perp^{R_x}(\vec{x})$	=	same as $b_\perp^{T_x}(\vec{x})$, but referring to the signal received
q	=	pulse moment = current $\times\Delta\tau$
$\Delta\tau$	=	pulse length
t	=	time elapsed since start of pulse
T_2^*	=	transverse relaxation time

The field $b_\perp^{T_x}(\vec{x})$ is equal to the physical field $B_\perp^{T_x}(\vec{x})$ (the component of the energizing magnetic induction field perpendicular to the Earth's magnetic field) divided by the current I through the loop. In Appendix A we discuss explicit expressions for the magnetic induction fields generated by a circular loop with radius a. We also give the higher order terms due to the residual frequency dependence in this field.

Before discussing the consequences of the generalized geometry for underground conditions, let us review some of the units pertinent to the calculation of the induced voltage. In view of the smallness of the signal it has become customary to express it in nV. Consequently the response E_d, which is discussed in Section 3, is expressed in nV/m. By using the units $[x^3] = \mathrm{m}^3$, ω_0

$= \mathrm{s}^{-1}$, $[M_0] = \mathrm{nT}$ (nano tesla), $[w(x)] =$ dimensionless with values between 0 and 1 (percentage water/100) and $[b_\perp^{R_x}(\vec{x})] = \mathrm{nT/A}$, we can immediately express $E(t)$ in nV. The dimensionless nature of the product $\gamma b_\perp^{T_x}(\vec{x})q$ follows from using the units $[\gamma] = 0.2657\ \mathrm{s}^{-1}\ \mathrm{nT}^{-1}$, $[q] = \mathrm{A.s}$, and the units for $b_\perp^{R_x}(\vec{x})$ mentioned above. For those familiar with nuclear physics units it is instructive to verify the relationship: $\gamma = 2g_p\frac{e\hbar}{2m_p}$, by converting to the units above.

The geometry of the current problem enters the expression for the voltage $E(t)$ via $b_\perp^{R_x}(\vec{x})$. In order to analyze the geometrical differences between the different cases, we will give some of the explicit formulae for the relative vectors. The relevant directions are those of the Earth's magnetic field, the orientation of the transmitter loop, and the orientation of the water layers. The Earth magnetic field can be expressed in terms of a right-handed coordinate system: $(\vec{e}_{North}, \vec{e}_{East}, \vec{e}_{down})$, where $\vec{e}_{down}$ is the opposite of the vertical pointing out of the Earth. Using the standard definitions of declination D and inclination I (Dobrin, 1976), one obtains the following expression for the normalized magnetic field :

$$\hat{B}_0 = \cos D \cos I\ \vec{e}_{North} + \sin D \cos I\ \vec{e}_{East} + \sin I\ \vec{e}_{down}\ . \tag{2}$$

Typical values of the D and I parameters in the mining area in South Africa are $D = -17^0$ (West) and $I = -63^0$ (Up). These values were obtained from (www.ngdc.noaa.gov/seg/geomag/, November 26, 2007) and refer to Johannesburg (latitude 25.5^0 South and longitude 27.5^0 East) and lead to $\hat{B}_0 = 0.439\ \vec{e}_{North} - 0.137\ \vec{e}_{East} - 0.888\ \vec{e}_{down}$. The estimated value of the magnetic field at any other point on Earth at any time can be found at the same website.

The circular loop gives rise to a magnetic field with components B_ρ and B_z (see appendix), where, the z and ρ-direction are defined in an axial coordinate system with the centre of the loop as origin, and the z-axis in the direction of the normal of the loop. The perpendicular field, now reads:

$$\vec{B}_\perp = B_\rho(\rho, z)\left[\hat{\rho} - (\hat{\rho} \bullet \hat{B}_0)\hat{B}_0\right] + B_z(\rho, z)\left[\vec{e}_z - (\vec{e}_z \bullet \hat{B}_0)\hat{B}_0\right]\ , \tag{3}$$

and the resulting magnitude of this field is given by:

$$\vec{B}_\perp^2 = B_\rho^2(\rho, z) + B_z^2(\rho, z) - \left[B_\rho(\rho, z)\ \hat{\rho} \bullet \hat{B}_0 + B_z(\rho, z)\ \vec{e}_z \bullet \hat{B}_0\right]^2\ . \tag{4}$$

We now have to connect the Earth magnetic and loop coordinate system, in order to calculate the voltages.

For the standard surface observations we assume the loop to be parallel to the surface of the Earth, i.e. the normal of the loop points into the Earth: $\vec{n} = \vec{e}_z = \vec{e}_{down}$. The ρ - vector is then given by:

$$\hat{\rho} = \cos\phi\ \vec{e}_{North} + \sin\phi\ \vec{e}_{East}\ . \tag{5}$$

where ϕ is the angular coordinate in the axial coordinate system, in this case measured from the North direction towards the East direction inside a plane with a normal along the down axis. The resulting magnitude of the perpendicular field, Eq.(4), can now be given more explicitly as follows:

$$\vec{B}_{\perp}^2 = B_{\rho}^2(\rho, z) + B_z^2(\rho, z) - \left[B_{\rho}(\rho, z)\cos(\phi - D)\cos I + B_z(\rho, z)\sin I\right]^2 \quad (6)$$

It is customary for the surface application to assume that the water layer is parallel to the surface, and thus also parallel to the loop. Furthermore one assumes that the water content $w(\vec{x})$ is independent of the direction ϕ for fixed z. After integrating the water content for a fixed z over all angles ϕ in Eq.(1), one finds that the voltage is independent of the declination D. Clearly, if these assumptions are not valid then the voltage will in general depend on D. Some MRS software exploits this special circumstance by only requiring the inclination I as input. When this whole setup is rotated, as we will do in the mine wall case, we can still use the same formulation, however, we must construct a modified inclination I' and declination D', which can be expressed in terms of I, D and the angles of rotation of the loop.

Let us now consider the mine wall case explicitly. We assume that the loop is placed against the mine wall, to minimize the distance between the loop and the potential water layers behind the wall, and that the water layer behind the wall is parallel to the loop. Hence, this situation is a pure rotation of the idealized surface case. The geometry can be expressed in terms of the vectors $\hat{\vec{B}}_0$ and $\vec{n}$. We want to express these vectors in the coordinate system that is used to define the Earth magnetic inclination and declination. To this end we characterize the normal to the loop by two angles α and β:

$$\vec{n} = \sin\beta\,(\cos\alpha\ \vec{e}_{North} + \sin\alpha\ \vec{e}_{East}) \ \ + \cos\beta\ \vec{e}_{down} \quad (7)$$

where $\beta = 0$ corresponds to the surface case, just discussed. We can obtain this vector from the original surface case by a rotation over β around the (positive) East direction, followed by a rotation over α around the (positive) down axis. Physically, this MRS geometry is equivalent to rotating the Earth magnetic vector in the opposite direction and leaving the normal to the loop in the z-direction. Hence, by rotating the Earth magnetic field by α degrees around the (negative) down axis, followed by a rotation of β degrees around the (negative) East direction we arrive back at the surface MRS geometry. The resulting magnetic vector is characterized by the equivalent inclination:

$$\sin I' = \cos I \sin\beta\cos(D - \alpha) + \sin I\cos\beta. \quad (8)$$

Not surprisingly $\sin I'$ equals the inproduct $\vec{n} \bullet \hat{B}_0$, which is the expression that controls the magnitude of the voltage as far as the geometry is concerned. This is due to the fact that under the given geometric assumptions the signal can only depend on the relative angle between the Earth magnetic field and the

normal of the loop plane. We see that the voltage is only independent of the magnetic declination D if $\beta = 0$ (the surface case) or if $I = \pm\pi/2$. The equivalent declination is given by:

$$\tan D' = \frac{\cos I \sin(D-\alpha)}{\cos I \cos\beta \cos(D-\alpha) - \sin\beta \sin I}. \tag{9}$$

This variable does not influence the amplitude under the idealized assumptions.

The normal orientation of the mine wall is vertical, i.e. its normal is in the horizontal plane. Since the loop normal is directed into the wall, $\beta = \pi/2$, while α determines the orientation of the wall and the half-space behind it. So we only have to specify one further parameter, namely α:

$$\sin I' \equiv \vec{n} \bullet \hat{B}_0 = \cos I \cos(D-\alpha). \tag{10}$$

In the mining area quoted above, $D = -17°$ (West) and $I = -63°$ (Up). Hence, the inproduct in the surface case is characterized by $\sin I = \sin(-63°) \approx -\frac{1}{2}\sqrt{3}$, while in the mine wall case it is characterized by $\cos I \cos(D-\alpha)$, whose magnitude is less than $\frac{1}{2}$. Since the perpendicular component $B_\perp^{R_x}(\vec{x})$ (which contributes towards the integral Eq.(1)) is small when the vectors $\vec{n}$ and $\hat{B}_0$ are close to parallel, a large inproduct implies a small signal (as far as the geometry is concerned). Thus, the surface case (almost parallel) generates a smaller voltage signal than the mine wall case, assuming other parameters to be equal. Hence, the largest signal occurs if $\alpha = D + \pi/2$, or when the Earth magnetic field vector lies inside the mine wall, while the smallest signal occurs if the declination and the normal of the loop coincide or are opposite. In the explicit calculations discussed in the next section we will see a confirmation of this qualitative assessment. The expectation that the mine wall signal would be enhanced for the relevant values of I, was one reason to engage in this feasibility study, despite the various negative factors.

Girard et al. (2008) and Rommel et al. (2006) have considered a more complex geometry, where the loop is positioned along a surface that slopes at low angles, while the water layer is still assumed to be horizontal. This geometry involves three independent vectors ($\vec{B}_0$, $\vec{n}$, and the normal to the water layer), while the symmetry in ϕ is lost as the water layer cannot extend above ground. Girard et al. (2008) propose some numerical approximation to replace the full integration by sublayers resembling the standard surface case, so that they do not have to carry out a full three dimensional integral.

3 Voltage response calculations under idealized mining conditions with synthetic data

We have simulated the response signal of an MRS experiment at three locations: Johannesburg (South Africa), Berlin (Germany) and Kirkland Lake (Ontario, Canada), with a particular emphasis on the different geometrical parameters. Two of these sites (South Africa and Canada) represent centres of mining activity, while several MRS tests have in the past been conducted near Berlin in Germany. The location and the characteristics of the geomagnetic fields (obtained using the igrf-2005 model (www.geomag.usgs.gov, November 26, 2007)) at these three places are given in Table 1 below. It is worth noting that the strength of the magnetic field is substantially higher in the given locations in the Northern hemisphere. In the case of the gold and platinum mines in South Africa, the rocks (quartzitic and anorthositic) are non-magnetic, so that we do not have to be concerned about negative effects on the signal strength, as described by (Keating and Knight, 2008).

Table 1
Characteristics of Simulation Sites

Location	Latitude	Longitude	B (nT)	Inclination	Declination
Johannesburg	26.5°S	27.5°E	28300	$-63°$	$-17°$
Berlin	52.5°N	13.0°E	49000	67°	2°
Ontario	48.0°N	81.0°W	57000	74°	$-11°$

In our calculations of response curves we started by verifying that our calculations agreed with the results given by Legchenko and Valla (2002). They do, provided we take proper account of the different conventions (also see appendix). Figure 1 shows the calculated response signals (the signal extrapolated back to $t = 0$, normalized per unit length of width) for a layer of water parallel to and 10 m from a circular loop of radius $a = 50$ m. Since typical water-bearing fractures are of the order of 50 cm wide, the actual signal received would be typically half of the numerical value shown. The value of $a = 50$ m is typical for surface experiments. For the mine wall case a value of $a = 1.5$ m would be more typical, however, the following analyses are still relevant for the mine wall case, as the enhancement factors only depend on the ratios z/a and ρ/a, which are independent on the overall scale. Later we will show amplitudes with more realistic magnitudes for the mine wall case when we consider the case $a = 1.5$ m in Table 2.

The surface case in Johannesburg corresponds to $I' = I = -63°$, where the signal is quite low (about 90 nV). The mine wall cases runs between $I' = I + \pi/2 = 27°$ for $\alpha = D = -17°$ and $I' = 0$ for $\alpha = D + \pi/2$. This corresponds to a range of signals between 110 and 120 nV. This confirms

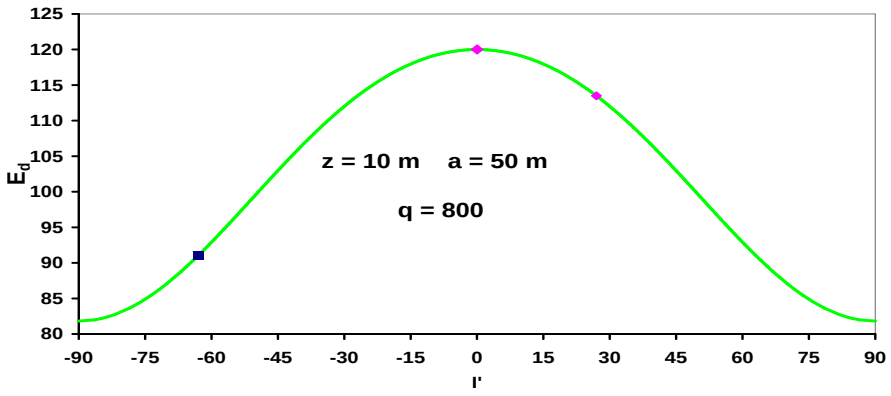

Fig. 1. Response signal amplitude in nV/m as a function of effective inclination (I') for B = 28300 nT, a loop radius of 50 m, q = 800 A.ms, and a 1 m thick water layer 10 m from the loop.

our initial expectation that the geometric factors favors mine-wall MRS over surface MRS. The enhancement ranges is around 30%.

In Fig. 2 we display the case for $z = a = 50$ m. The three special values of I' considered above remain the same, however, the value of q for which the first maximum is reached varies considerably. Hence, it makes little sense to display the different I' results for the same q as we did in Fig. 1, and we have chosen to display the results for the value of q where the signal is first maximal. These maximum pulse moment values are shown later on in Fig. 3. The pattern in Fig. 2 is very different from that in Fig. 1, The maximum near $I' \approx 0$ is no longer so prominent, while the results near $\pm 90^0$ now represent maxima, rather than minima. For explaining this phenomenon we have to discuss the contributions to the perpendicular magnetic field $B_\perp^{T_x}(\vec{x})$ in some detail. Our qualitative argument for expecting that the pattern in Figure 1 would be dominant, is that the perpendicular magnetic field would be large if $\vec{n} \bullet \hat{B}_0$ is small, in other words when I' is small. This was indeed the case for Figure 1. However, by examining Eq.(6) we see that this argument only works properly if B_ρ dominates over B_z, since in this case $\vec{B}_\perp^2 = B_\rho^2 \cos^2 I' \approx B_\rho^2$, where we tacitly replaced I by the effective parameter I'. If B_z dominates over B_ρ then $\cos I \approx 0$ leads to a maximal expression, so that we get a maximum near $I' = \pm\ 90^0$. The first case applies for small z, while the latter applies for large z. This explains the behavior in Fig. 2 qualitatively. But this also means that the enhancement we counted on for the mine wall case is not realized for the more interesting large z case. In fact the signal in the surface case (31.3 nV) is slightly larger than the one in the mine-wall case (corresponding to values

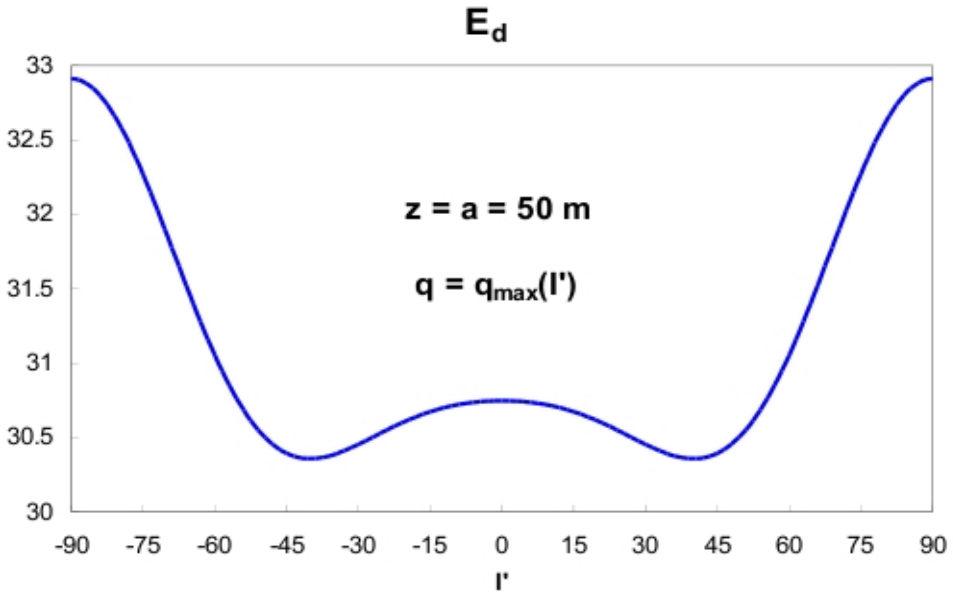

Fig. 2. Maximum signal amplitude as a function of effective inclination (I') for $B = 28300$ nT, a loop radius of 50 m, and a 1 m thick water layer 50 m from the loop. The amplitude is determined at $q_{\max}$ defined in Figure 2.

between 30.5 and 30.8 nV), although the differences are rather minimal. From the results shown in Table 1 we see that for $z >> a$ the roles are inverted again, and the mine-wall case is enhanced once again over the surface case.

In Figure 3 we show the dependence of q_{max} on I'. In the case considered ($z = a = 50$ m), the required pulse moment is much larger in the surface case (5356 As) than in the mine-wall case ($3742 - 4025$ As). This may be considered as a slight advantage for carrying out MRS experiments underground.

Table 2 shows the amplitudes E_d at the value q_{max}, for which the signal reaches its first maximum. We display a range of z-values (as usual z corresponds to a layer of water parallel to the loop and z meters from the loop). The difference in the maximum value of E_d between the vertical and horizontal loops is larger for relatively small values of z. This difference is also larger where the magnetic field itself is stronger. Thus we find that for $z = 5$ m and a loop size of 50 m the maximum amplitude for the vertical loop is $1.42, 1.48$ and 1.54 times larger than that of the horizontal loop for the South African, German and Canadian cases respectively. As the values of z approach the radius of the loop a the maximum amplitude of the signal decreases and the difference between the vertical and horizontal cases becomes negligible. At $z = 20$ m the differences in signal strengths are of the order of 3%.

For the smaller loop (in the table we have used a radius of 1.5 m) the signal

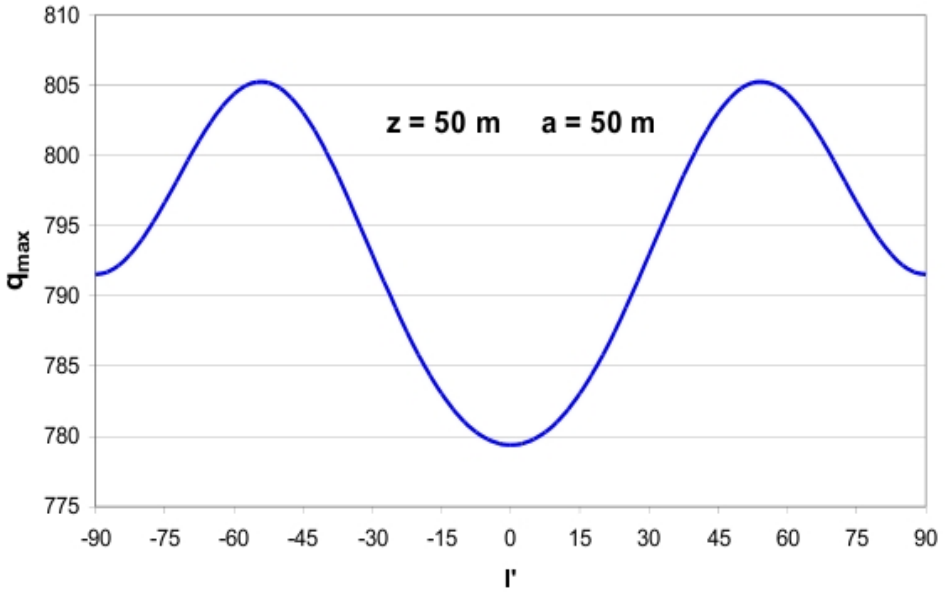

Fig. 3. Maximum impulse moment (the value of q for which the amplitude reaches its first maximum) as a function of the effective inclination (I'), for $B = 28300$ nT, a loop radius of 50 m and a 1 m thick layer of water 50 m from the loop.

Table 2
Maximum amplitudes of MRS response curves in nV/m for horizontal and vertical case with $I' = 0$. The values in brackets are the impulse moments q_{max} for which the first maximum is obtained. Units are as usual A.ms

		Johannesburg		**Berlin**		**Ontario**	
a [m]	z [m]	Horizontal	$I' = 0$	Horizontal	$I' = 0$	Horizontal	$I' = 0$
50	5	102 (410)	145 (474)	290 (405)	437 (474)	371 (397)	609 (474)
	10	91 (803)	120 (774)	261 (799)	355 (774)	339 (797)	478(774)
	20	69 (1603)	76 (1283)	203 (1627)	223 (1283)	270 (1662)	302 (1283)
	50	31.3 (5392)	30.8 (3742)	93.3 (5583)	90.9 (3742)	128.0 (5884)	122.5 (3742)
	100	9.8 (20750)	12.3 (14838)	28.8 (21644)	36.2 (14838)	38.7 (23174)	48.8 (14838)
1.5	0.5	2.3 (40)	2.6 (33)	6.6 (40)	7.7 (33)	8.8 (41)	10.4 (33)
	1	1.44 (88)	1.43 (64)	4.28 (90)	4.22 (64)	5.82 (94)	5.68 (64)
	1.5	0.94 (162)	0.92 (112)	2.80 (168)	2.73 (112)	3.84 (177)	3.67 (112)
	2	0.63 (270)	0.65 (188)	1.86 (281)	1.93 (188)	2.55 (298)	2.60 (188)

strength for meaningful z-values is already very small. In the South African case the maximum amplitude generated by a layer of water 1 m from the loop is already less than 2 nV and the orientation of the loop makes no practical difference. In the other locations, where the magnetic field is stronger, the maximum amplitude with identical settings is between 4 and 6 nV, but again the difference between the signal derived from the horizontal and vertical loops

is not meaningful.

4 In-mine experiments

To test the feasibility of the underground usage of MRS, underground tests were performed. We used an NMR system designed and manufactured by Radic Research of Germany for application to shallow surface based investigations. This SNMR MIDI 3-channel instrument has been successfully tested with a T_x loop as small as 1 m diameter (Radic, 2007) which makes it ideal for underground tests where space restrictions limit the size of T_x loops. To more effectively suppress cultural electromagnetic noise, of which high levels were anticipated underground, a Remote Reference Technique (RRT) is utilized (Radic, 2007). The RRT method consists of two smaller (1 m x 1 m) orthogonal receiver loops that measure noise before and during a MRS. A multivariate coherence analysis method is used to calculate the magnetic transfer function needed to predict and eliminate the noise recorded in the Free Induction Decay (FID) record. This has the advantage of reducing the conventional stacking time and should improve measurement efficiency and S/N ratio. A 3 m x 3 m T_x/R_x coil was constructed for the underground tests. By using this coil with 128 turns, we were able to obtain equivalent pulse moments to those of a 10 m x 10 m coil with 12 turns normally used during surface based MRS. Two channels are used for the RRT, while the third channel is used for signal recording (Meyer et al., 2007).

Two underground tests have been conducted during these trials. The tests at both experimental locations were done under very difficult conditions. Apart from the limited space available to use a larger loop diameter, high temperature ($50°C$) and close to 100% humidity conditions, mining operations throughout the entire mine could not be interrupted for the duration of our tests. This we believe further contributed to the already high noise levels. Due to the poor S/N ratios, the signal recording channels were saturated and real signal could not be separated from the noise. None of the mine experiments provided results where signals could be clearly separated from noise, and thus we prefer to limit ourselves to some general statements on the in-mine experiments.

The first experiment was at the Modikwa Platinum Mine in the Eastern Bushveld Complex at a depth of about 150 m below surface, while the second was at Tau Tona Gold Mine in the Western Witwatersrand Gold Mining District, some 2.9 km below surface. Excessive electromagnetic noise was encountered at Modikwa Mine that resulted in saturation of the different receiver channels. The excessive noise is believed to have originated from ongoing mining activity at levels above and below the mining face where our experiments

were conducted. Noise amplitudes measured by the vertical orthogonal RRT coils were about 1.5 V. At Tau Tona Mine the observed noise levels were also far above the theoretically calculated and expected signal amplitudes. However, the noise experienced at this deeper experimental site, was significantly lower than at Modikwa Mine despite continued mining activities relatively close to the test site.

The relatively low noise experienced at the 2 900m depth experimental site is partly attributed to attenuation by the overlying highly resistive quartzite rocks present in the Witwatersrand gold fields. According to formulae given by King and Smith (1981) and Vogt (2000 to calculate attenuation, the attenuation using a rock resistivity of 10 000 ohm.m and a dielectric constant of 10 at a frequency of 1200 Hz (the Larmor frequency at the local Earth magnetic field strength) amounts to 0.00069 Neper/m or 0.006 dB/m. At a depth of 2 900 m below surface a 17.3 dB attenuation of the noise level experienced on surface can be expected. Using the same rock properties, an attenuation of only 0.89 dB could be expected at the shallower experimental site in the Modikwa Platinum Mine. Lower noise levels experienced in the deep gold mine experimental site are therefore in part attributed to the attenuation of electromagnetic noise by the thick cover of highly resistive mainly quartzitic rock.

5 Summary and Discussion

In this paper we considered the feasibility of underground applications of MRS. Our particular interest was the detection of the water content of waterbearing fractures ahead of mining operations. We anticipated that the inhibiting circumstances (small loop size, high electromagnetic noise, low water content in secondary aquifers) would be partially offset by favorable geometric conditions in mining areas. We investigated this possibility by identifying the dependence of the effective inclination (which characterizes the geometric dependence of the MRS signal) on the Earth magnetic inclination and declination, and two other parameters that characterize the orientation of the mine wall. We found that the signal enhancement (about 30%) was present for small depths (i.e. for small values of z/a), but was not significant at the larger depths required for mining circumstances. This indicates that this application of underground MRS is barely feasible in Southern Africa with the currently available technology. In Canada and Europe this application is slightly more feasible, because of the stronger Earth magnetic field in the areas of interest,although the signal would still be very small. Another possible application exists for tunnel excavations in mountainous areas. In such a case slightly larger loops can be envisaged, thereby enhancing the signal.

We have extended the usual signal formula to include terms that are higher order in the wave number and presented them in an easily calculable format. Such terms become important if the rocks display high conductivity and if one is interested in large depth ratios z/a. We anticipated that these terms could play an important role in the underground applications, since the constraints on the loop size (small a) forces one to consider large z/a - ratios. Due to the high resistivity of rocks in South Africa the relevance of these terms is low in this case, however, where the resistivity of rocks is lower, these terms already play a role for moderate depths ($z \approx 2a$). In surface applications these terms may play a role because the signal amplitude is larger than in the underground case (large a), so that the higher order corrections to the signal already could be measurable at moderate values of z/a, so that their inclusion could improve the accuracy of MRS analyses.

A Computation of the applied field

In the NMR application we assume that the applied field is generated by a circular loop, the same assumption as made by Legchenko and Valla (2002). These authors represent the magnetic field as a product of a real time independent amplitude and an oscillatory exponential function. Below we show that the amplitude after extracting the oscillatory exponential function contains an additional frequency dependence, which can fairly easily be incorporated in the calculations. Instead of real, this amplitude is now complex, although to third order in the frequency we can represent it by a real amplitude.

The current is represented as follows (Jackson, 1975, p. 177):

$$\vec{J} = (-\vec{i}\ \sin\phi + \vec{j}\ \cos\phi) J_\phi\ , \tag{A.1}$$

$$J_\varphi(\vec{x},t) = I\ \exp(-\mathrm{i}\omega t)\ \sin\vartheta\ \delta(\cos\vartheta)\ \frac{\delta(r-a)}{a}\ . \tag{A.2}$$

The resulting vector potential equals (combine Eqs. (6.52), (6.54) and (6.69) in Jackson (1975)):

$$\begin{aligned}\vec{A}^{(\pm)}(\vec{x},t) &= \frac{1}{c}\int \mathrm{d}^4x'\ \vec{J}(\vec{x}',t')\frac{\delta\left(t' - \left[t \mp \frac{|x-x'|}{c}\right]\right)}{|x-x'|} \\ &= (-\vec{i}\ \sin\phi + \vec{j}\ \cos\phi) A_\phi^{(\pm)}(\rho,z,t)\ .\end{aligned} \tag{A.3}$$

The retarded solution ($A_\phi^{(+)}$) is:

$$A_\phi(\rho,z,t) \;= -\frac{4Ia}{c}\exp(-\mathrm{i}\omega t)\int\limits_0^{\pi/2}\mathrm{d}\psi\;\cos(2\psi)\frac{\exp(\mathrm{i}kR(a,\rho,z,\psi))}{R(a,\rho,z,\psi)} \qquad \text{(A.4)}$$

where we replaced ω/c by the wave number k and introduced the short hand notation:

$$R(a,\rho,z,\psi) = \left[(\rho+a)^2+z^2-4\,\rho\,a\,\sin^2\psi\right]^{1/2}\;. \qquad \text{(A.5)}$$

To verify this derivation one might want to consult Jackson (1975), who provides an intermediate result in the static case (see his Eq.(5.36)).

In a conductive medium we have to add a conductive contribution to the wave number (Jackson, 1975, p. 296):

$$k^2 \to k'^2 = k^2(1+\frac{4\mathrm{i}\pi\sigma}{\varepsilon\omega})\;. \qquad \text{(A.6)}$$

An equivalent expression is used by (Weichman et al., 2000). Normally, the conductivity σ is expressed in units of siemens/m, while the value of ε in vacuum (ε_0) equals $(8.85418782 \pm 7) \times 10^{-12}$ in units of F/m. This gives the ratio σ/ε in units of s^{-1}. In typical cases relevant for the current application ($\sigma \approx .001$ S/m and $\omega \approx 7500\ \mathrm{s}^{-1}$) the second term is nearly 0.2 million times as big as the first term. In this case we can approximately set $k' \approx k(1+i)\sqrt{2\pi\sigma/\epsilon\omega}$, so that $k' \sim \omega^{1/2}$. Most treatises of MRS limit themselves to the zeroth order term in k', i.e. they ignore any k'-dependence. This would generally be justified for non-conductive media. However, for conductive media this is a dubious assumption. At the end of this appendix we will show at which distances z the higher frequency terms become as important as the standard zeroth order term. We will demonstrate that the second order correction can also be expressed in elliptic integrals and thus can be evaluated fairly easily (the first order term vanishes). The third order term can even be calculated analytically. The expansion now looks like:

$$\begin{aligned} A_\phi(\rho,z,t) = \frac{4Ia}{c}\exp(-i\omega t)\Bigg[&\int\limits_0^{\pi/2}\mathrm{d}\psi\;\cos(2\psi)\frac{1}{R(a,\rho,z,\psi)} \\ &-\frac{k'^2}{2!}\int\limits_0^{\pi/2}\mathrm{d}\psi\;\cos(2\psi)R(a,\rho,z,\psi) - \mathrm{i}\frac{k'^3}{3!}\frac{\pi\rho a}{2} + \mathrm{O}(k'^4)\Bigg]. \end{aligned} \qquad \text{(A.7)}$$

The advanced solution ($A_\phi^{(-)}$) only starts differing from the retarded solution

in the third order term (its sign is then opposite to that in Eq.(A.7)). The advanced solution applies to the signal received by the loop. For a conductive medium, the second order term becomes complex, with the imaginary part being proportional to the conductivity. The magnetic fields generated by the loop can be expressed in terms of this vector potential:

$$B_z = \mu \left\{ \frac{A_\phi}{\rho} + \frac{\partial A_\phi}{\partial \rho} \right\} \quad \text{and} \quad B_\rho = -\mu \frac{\partial A_\phi}{\partial z} \ , \tag{A.8}$$

where μ is the magnetic permeability. It has become customary to rewrite the first term in (A.7) in terms of elliptic integrals, a result that carries through in the magnetic fields. We will extend this procedure to the second order term. Introducing the short-hand notation:

$$m^2 = \frac{4a\rho}{(\rho + a)^2 + z^2} \ , \tag{A.9}$$

we have up to third order in k':

$$\begin{aligned} A_\phi(\rho, z, t) = \frac{4Ia}{c} e^{-\mathrm{i}\omega t} \Bigg[& \frac{m}{\sqrt{4\rho a}} \left\{ \left(1 - \frac{2}{m^2} \right) K(m) + \frac{2}{m^2} E(m) \right\} \\ & - \frac{k'^2}{2!} \frac{\sqrt{4\rho a}}{m} \left\{ \frac{2}{3} \left(1 - \frac{1}{m^2} \right) K(m) + \frac{1}{3} \left(\frac{2}{m^2} - 1 \right) E(m) \right\} \\ & - \frac{k'^3}{3!} \frac{\pi \rho a}{2} \Bigg] , \end{aligned} \tag{A.10}$$

where the elliptic integrals are defined by

$$K(m) = \int_0^{\pi/2} \mathrm{d}\psi \ \frac{1}{\sqrt{1 - m^2 \sin^2 \psi}} \ . \tag{A.11}$$

and

$$E(m) = \int_0^{\pi/2} \mathrm{d}\psi \ \sqrt{1 - m^2 \sin^2 \psi} \ . \tag{A.12}$$

The only new identity for elliptic integrals which is not given in the standard literature and is needed for this derivation is:

$$\int_0^{\pi/2} \mathrm{d}\psi \ \cos 2\psi \sqrt{1 - m^2 \sin^2 \psi} = \frac{2}{3}(1 - \frac{1}{m^2})K(m) + \frac{1}{3}(\frac{2}{m^2} - 1)E(m) \ . \tag{A.13}$$

The magnetic fields can then also be expressed in terms of elliptic integrals using Eq.(A.8) and the relationships:

$$\frac{\partial K}{\partial m} = \frac{E}{m(1-m^2)} - \frac{K}{m} \quad \text{and} \quad \frac{\partial E}{\partial m} = \frac{E}{m} - \frac{K}{m} \; . \tag{A.14}$$

We find:

$$\begin{aligned} B_z(\rho,z,t) = 2I\mu \frac{\exp(-\mathrm{i}\omega t)}{\{(a+\rho)^2+z^2\}^{1/2}} \Bigg[& K(m) + \frac{a^2-\rho^2-z^2}{(a-\rho)^2+z^2} E(m) \\ & + \frac{k'^2}{2!}\Big\{K(m)(a^2-\rho^2-z^2) + E(m)(a^2+2a\rho+\rho^2+z^2)\Big\} \\ & + \frac{\mathrm{i}k'^3}{3!}\pi a^2 \{(a+\rho)^2+z^2\}^{1/2}\Bigg] \; , \end{aligned} \tag{A.15}$$

and

$$\begin{aligned} B_\rho(\rho,z,t) = \frac{2I\mu z}{\rho} \frac{\exp(-\mathrm{i}\omega t)}{\{(a+\rho)^2+z^2\}^{1/2}} \Bigg[& -K(m) + \frac{a^2+\rho^2+z^2}{(a-\rho)^2+z^2} E(m) \\ & + \frac{k'^2}{2!}\Big\{K(m)(a^2+\rho^2+z^2) - E(m)(a^2+2a\rho+\rho^2+z^2)\Big\}\Bigg] \; . \end{aligned} \tag{A.16}$$

One can easily show that up to a factor 4π (choice of dimensional units) the zeroth order results agree with Legchenko and Valla (2002). The permeability μ can be used to connect the different systems of units. For the vacuum we have $\mu = 4\pi \times 10^{-7}$ [H/m] = [tesla m A^{-1}].

The higher order terms are important for conductive media and larger distances z. In the South African case the conductivity is very low underground ($\sigma = 0.001$ S/m) and the Earth magnetic field is roughly $28,000$ nT. This means that $|k'| \approx 0.01\ m^{-1}$. Analyzing B_z one finds that the second order term reaches the same magnitude as the zeroth order term for $z \approx 3a$, while the third order term only catches up at $z \approx 7a$. However, if $z \approx 3a$ then B_ρ dominates B_z by a factor of 6 approximately, so the behavior of B_ρ is more relevant. We find that for B_ρ the second order term only comes into play at $z \approx 6a$, at which distance the signal has weakened considerably. In a more conductive environment, with $\sigma = 0.1$ S/m, we find $|k'| \approx 0.1\ m^{-1}$. In this case the second order term already becomes important (for B_z) when $z \approx a$, and the dominance of B_ρ over B_z at this value of z is also less, namely about a factor 2. For B_ρ the second order term comes into play for $z \approx 2.5a$, so

clearly in this case it seems worth while to consider the higher order terms. The fact that these terms are of similar (absolute) magnitude as the zeroth order term for the z-values mentioned does not necessarily mean that they lead to an enhancement, as they are generally complex and can either act as constructive or destructive terms.

Acknowledgements

The authors acknowledge the support provided by Michael van Schoor of the CSIR. The second author is grateful to Jean Roy and Gerhard Lange for discussions about the concept of using MRS in mining applications. We wish to thank Tau Tona Gold Mine and Modikwe Platinum Mine for allowing us to perform the underground trials at their facilities, and Tino Radic of Radic Research for providing the testing equipment.

References

Dobrin, M., 1976. Introduction to Geophysical Prospecting. McGraw-Hill.

Girard, J.-F., Legchenko, A., Boucher, M., Baltassat, J.-M., 2008. Numerical study of the variations of magnetic resonance signals caused by surface slope. Journal of Applied Geophysics 66, 94–103.

Jackson, J. D., 1975. Classical Electrodynamic. John Wiley and Sons, New York.

Keating, K., Knight, R., 2008. A laboratory study of the effect of magnetite on nmr relaxation rates. Journal of Applied Geophysics 66, 188–196.

King, R. W. P., Smith, G. S., 1981. Antennas in Matter. The MIT Press, Cambridge, Massachusetts.

Lange, G., Yaramanci, U., 2005. Handbuch zur Erkundung des Untergrundes von Deponien, Band 3, Geophysik. Springer, Berlin, Ch. Oberflachen-Nuklear-Magnetische Resonanz, p. 1102.

Legchenko, A., Baltassat, J.-M., Beauce, A., Bernard, J., 2002. Nuclear magnetic resonance as a geophysical tool for hydrogeologists. Journal of Applied Geophysics 50 (1-2), 21–46.

Legchenko, A., Valla, P., 2002. A review of the basic principles for proton magnetic resonance sounding measurements. Journal of Applied Geophysics 50 (1-2), 3–19.

Lubczynski, M., Roy, J., 2004. Magnetic resonance sounding: New method for ground water assessment. Ground Water 42, 291–303.

Meyer, R., van Schoor, M., Greben, J., 2007. Development of and tests with the MRS technique to detect water bearing fractures. In: Linzer, L., Vogt, D.

(Eds.), Proceedings of the 10th SAGA Biennial Conference and Exhibition 'Making Waves', KwaZulu Natal, South Africa.

Radic, T., December 2007. Nuclear Magnetic Resonance (NMR) Instrumentation. SNMR MIDI. Radic Research, www.radic-research.de.

Rommel, I., Hertrich, M., Yaramanci, U., 2006. The effect of topography on MRS measurements with separated loops. In: Proceedings, MRS2006, Madrid, Spain.

Roy, J., Lubczynski, M., 2003. The magnetic resonance sounding technique and its use for groundwater investigations. Hydrogeology Journal 11, 455–465.

Schweitzer, J. K., Stephenson, F. P., 1999. Borehole drilling and behaviour at great depths, Part 1. Deepmine Collaborative Research Project. Tech. Rep. RR99-0210, CSIR Miningtek, Johannesburg, South Africa.

Semenov, A. G., 1987. NMR Hydroscope for water prospecting. In: Proc. Seminar on Geotomography. Indian Geophysical Union, pp. 66–67.

Varian, R. H., 1962. Ground liquid prospecting method and apparatus. Tech. rep., US Patent 3 109 383.

Vogt, D. R., 2000. The modelling and design of radio tomography antennas. Ph.D. thesis, University of York.

Weichman, P., Lavely, E. M., Ritzwoller, M., 2000. Theory of surface nuclear magnetic resonance with applications to geophysical imaging problems. Phys. Rev. E 62, 1290–1312.

Weichman, P. B., Lun, D. R., Ritzwoller, M. H., Lavely, E. M., 2002. Study of surface nuclear magnetic resonance inverse problems. Journal of Applied Geophysics 50 (1-2), 129–147.

Wolmarans, J. F., 1986. Some engineering and hydrological aspects of mining on the West Wits Line. In: Anhaeusser, C. R., Maske, S. (Eds.), Mineral Deposits of Southern Africa, Volume 1. Geological Society of South Africa, Johannesburg.

www.geomag.usgs.gov, November 26, 2007.
URL `geomag.usgs.gov`

www.ngdc.noaa.gov/seg/geomag/, November 26, 2007.
URL `www.ngdc.noaa.gov/seg/geomag/`

Yaramanci, U., Lange, G., Hertrich, M., 2002. Aquifer characterisation using surface NMR jointly with other geophysical techniques at the Nauen/Berlin test site. Journal of Applied Geophysics 50 (1-2), 47–65.